ACS OMEGA

http://pubs.acs.org/journal/acsodf

Article

Numerical Simulation of the Flow Pattern of Spiral Annular Flow with a Guide Strip by Spiral On-Way

Yongchao Rao, Shuli Wang,* and Lijun Li

Cite This: *ACS Omega* 2022, 7, 31961−31973

Read Online

ACCESS | Metrics & More | Article Recommendations

ABSTRACT: To study the gas−liquid two-phase spiral annular flow pattern and its conversion law in a horizontal tube with twist tape by spiral on-way, a numerical simulation is carried out using the RNG k-ε model, and the DPM model is adopted as the particle motion model. The research results show that three main flow patterns are obtained, which are spiraling churn flow, spiraling annular flow, and spiraling annular twine flow. The ratio of the liquid-phase to gas-phase velocity V_L/V_G is the main factor that affects the existence of the gas phase. When $V_L/V_G > 1/2$, the flow pattern is a spiral cluster flow; when $1/5 < V_L/V_G < 1/2$, the flow pattern is a spiral annular flow; and when $V_L/V_G < 1/5$, the flow pattern is a spiral annular flow. Compared with the flow pattern of the local spiral flow pattern of the short twisted band, it was found that the occurrence conditions of annular flow were postponed and a new flow pattern appeared. The research results of this paper have guiding significance for the pipeline risk management of natural gas hydrates and the engineering application of the full rotation of guide strips.

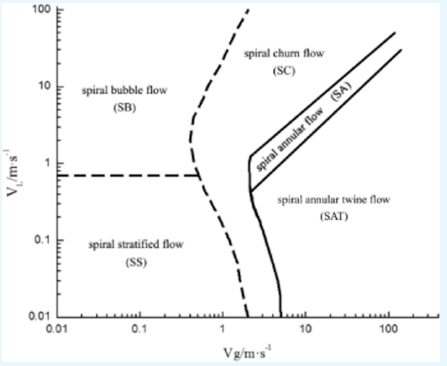

INTRODUCTION

Annular flow is a typical gas−liquid two-phase flow state that often occurs in many industrial applications. It is used to improve the heat and mass transfer efficiency, reduce heat loss, and improve the transportation efficiency due to its small liquid film flow rate, low kinetic energy consumption, low power consumption, and high mass transfer coefficient and heat flux. Moreover, the advantages of part of the spiral flow can be retained by the annular flow with spiral rotation, such as high shear force and strong particle-carrying capacity.

Slug flow[1] is also one of the common flow patterns in mixed transportation pipelines, and it occurs when the pipeline system is running normally, starting, stopping transportation, cleaning the pipeline, and adjusting the transportation quantity. Because of its strong intermittence and high pressure drop, slug flow is a typical transient flow. Therefore, long-term slugging transportation will damage the separation and treatment facilities downstream of the pipeline transportation system. However, unlike a typical continuous flow, annular flow will not have these problems. This is because the liquid forms an annular liquid film on the wall of the pipeline, and there is a continuous air channel in the center of the pipeline, in which the gas carries fine droplets and flows at a high speed. Because the annular flow in the horizontal pipe is influenced by gravity, the liquid film is asymmetrically distributed with a thick bottom and a thin top. The liquid interface is affected by high-velocity gas to generate a disturbance wave, and the gas keeps sucking the liquid droplets from the liquid film, while the liquid droplets keep splashing and settling back into the liquid film to cause secondary carrying. Therefore, the annular flow in a horizontal circular tube presents randomness, complexity, and asymmetry of liquid film thickness[2] due to its unique liquid film structure and flow characteristics. This extremely complicated and random situation should be avoided during pipeline transportation so as to prevent the downstream separation and treatment facilities from being adversely affected. Therefore, a device capable of inducing uniform annular flow is needed; this experimental goal can be better achieved by the spiral flow pipeline rotating through the impeller, the tie, and the guide strip. Therefore, the spiral flow can be stably converted into annular flow.

Zhou et al.[3] used the CLSVOF method to study the influence of the spiral diameter and the helix angle of the rectangular spiral pipe on the flow transition boundary and plotted the flow pattern map of different spiral diameters and different spiral angles. Wang et al.[4] conducted an experimental study on the gas−liquid two-phase spiral flow pattern with impeller rotation and analyzed the influence of different blade areas and angle convections on the pattern. Rao et al.[5] conducted an experimental study on the gas−liquid two-phase

Received: May 11, 2022
Accepted: August 12, 2022
Published: August 30, 2022

ACS Publications

© 2022 The Authors. Published by American Chemical Society

spiral flow pattern in a horizontal tube under a surfactant and found that SDBS can advance the transition boundary of the spiral annular flow, the spiral agglomerate flow, and the spiral dispersion flow. Cai et al.[6] found that the screw spiral channel to the annular flow region increases, while the intermittent flow region decreases. Liu et al.[7] conducted an experimental study on the flow characteristics of slug flow in a horizontally placed rectangular-section spiral channel. It was found that the combined action of gravity and centrifugal force affected the development of the liquid film and gave the law of liquid film change at different times. Liu et al.[8] used RSM and the VOF model to simulate the gas−liquid two-phase flow pattern of an ordinary straight tube. The results show that the model can be used to simulate bubble flow, stratified flow, wavy flow, slug flow, and annular flow. The flow and simulation results are in good agreement with the Mandhane flow pattern map. Cui et al.[9] used R134a as the working fluid to experimentally study the boiling gas−liquid two-phase flow pattern and pressure drop characteristics in a microfin spiral coil and obtained layered wave flow, intermittent flow, and annular flow. With the steam flow as the abscissa and the mass flow of the two phases as the ordinate, the flow pattern map is obtained, and the flow conversion formula and pressure drop formula are given. Subhashini and Nigam[10] studied the effect of the gas-bearing rate on flow patterns in spiral flow heat exchangers. The experiment obtained stratified flow, slug flow, plug flow, wave flow, and agitation flow. Based on the experimental results, the flow pattern map was drawn, and the empirical relationship among stratified flow, the transition zone, and the turbulent void fraction was established and compared with the results of Lockhart−Martinelli and Hughmark. Liu et al.[11] used high-speed flow visualization to experimentally study the gas−water two-phase flow characteristics in a vertical spiral rectangular channel. The flow pattern map of the spiral rectangular channel is given, the evolution process of the flow pattern at different positions of the spiral rectangular channel is expounded, and the coalescence problem of the bubble and the slug is discussed. Fabio and Gherhardt[12] studied the gas−liquid two-phase flow with a twist tape and obtained a total of five types of flow patterns: stratified flow, intermittent flow, annular stratified flow, annular flow, and plug flow. A new method is proposed to predict the pressure drop of the gas−liquid two-phase spiral flow. Wang et al.[13] studied and mastered the spiral flow characteristics in surfactant systems, and the flow pattern of the gas−liquid two-phase spiral flow under the surfactant system was divided into spiral linear flow, spiral wave stratified flow, spiral axial flow, and spiral dispersed flow. The effects of flow pattern, gas content, vane parameters, surfactant concentration, and flow rate on pressure drop were systematically investigated. Wang et al.[14−17] also conducted an exploratory study on gas−liquid two-phase flow patterns and studied the flow pattern and flow pattern transition boundary of gas−liquid two-phase spiral flow with vane and twisted types. Liu et al.[18,19] investigated the axial development of air−water annular flow with a spiral vane in a vertical pipe. A visualization experiment was carried out to investigate the flow patterns, void fraction, and pressure drop along the streamwise direction in the spiraling annular flow.

Cui et al.[20] experimentally studied the flow and heat transfer performance of refrigerant R134a in a three-dimensional microribbed spiral tube for the first time. It was found that when the mass flow rate was more than 100 kg/s, annular flow began to appear in the spiral tube. Zeng et al.[21] used FLUENT simulation software to simulate the annular flow of oil and gas in a pipe. It was found that gas velocity is the main factor affecting the quality of annular flow. When the oil amount is constant and the gas velocity is 60−80 m/s, annular flow has the best quality. Fang et al.[22] studied the flow characteristics of gas−liquid two-phase flow in a horizontal tube through a spiral vane by numerical simulation, and they carried out an experimental study of the nonintrusive measurement of phase separation and flow rate in the tube by trial-producing spiral vanes, and the error was controlled within 10%. Rao et al.[23] performed an experiment on gas−liquid two-phase spiral flow with the addition of the surfactant SDBS using a self-built circular spiral flow experimental platform and found that the surfactant SDBS changes the tension of the gas−liquid interface, which promotes the formation of spiral annular flow and spiral dispersion flow at a lower gas−liquid velocity. Kanizawa et al.[24] experimentally studied gas−liquid two-phase flow with a twisted tape, discussed the influence of different flow patterns on the pressure drop, and proposed a new method to predict the pressure drop of gas−liquid two-phase spiral flow with a twisted tape. Raeiszadeh et al.[25] designed a transparent vertical spiral pipe, analyzed the flow pattern conversion of gas−liquid two-phase spiral flow vertically downward using image processing technology, and compared the experimental results with the published vertical flowchart. It was found that pipeline rotation has a great influence on the transition boundary of the flow pattern; increasing the rotation of the pipeline will lead to early transition between slug flow and annular flow at a low gas velocity. Baghernejad et al.[26] studied the influence of a spiral pipe on pressure drop and the flow pattern transition boundary; they found that rotation has a significant effect on the convective transform boundary, and there is a smooth stratified flow in the horizontal pipe. With the increase in pipe rotation, the area where laminar flow appears decreases and even disappears at a high rotation speed. In addition, with the increase in pipe twist, the area of annular flow increases, while the pressure drop increases significantly with the increase in pipe rotation. For the inclined pipeline, the pressure drop is affected by both the torsional strength and the inclination angle of the pipeline, but with the increase in the torsional rate, the influence of the inclination angle of the pipeline on the pressure drop becomes smaller and smaller. Liu et al.[27] studied the effect of spiraling flow on the transition from lumpy flow to annular flow in a medium-diameter pipeline through experiments and modeling and found that the lumpy flow could be transformed into spiraling annular flow under the action of spiraling flow, and the gas velocity required for the transition from lumpy flow to annular flow with helical flow is lower than that without helical flow.

However, at present, research on spiral flow in a pipeline mostly uses local spinners, such as short twisted tapes[28] and impellers,[29] to generate spiral flow, which attenuates quickly, so many relays need to be installed for long-distance pipeline applications. There is little research on the entire spinning process. Therefore, this paper aims at two typical problems of natural gas hydrate pipeline flow: two-phase flow dominated by the gas phase and the liquid phase, and the spiral flow generated by the whole rotation of the guide strip. The flow and settling law of hydrate particles are studied, and the phase distribution and flow pattern change of gas−liquid two-phase spiral flow are discussed, which provides a theoretical basis and technical guidance for the safe transportation of natural gas hydrate by spiral flow.

https://doi.org/10.1021/acsomega.2c02924
ACS Omega 2022, 7, 31961−31973

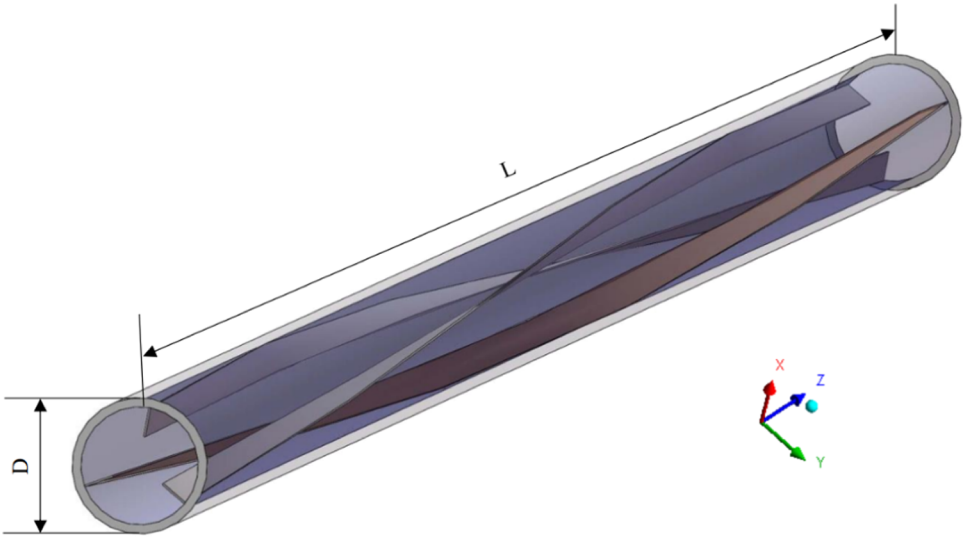

Figure 1. Geometric model.

NUMERICAL SIMULATION METHOD

Determination and Simplification of the Model. In the submarine gas pipeline, the extracted natural gas will carry drilling fluid and seawater, and the water in it will form hydrate particles with the natural gas at high pressures and low temperatures. Because the particle density of natural gas hydrates is close to that of water, but different from that of natural gas, natural gas hydrates and water can be regarded as a liquid phase together. The model is simplified as gas−liquid two-phase flow. In this paper, the simulation of the spiral annular flow pattern ignores hydrate particles and only considers the change in the flow pattern. This paper mainly studies the variation characteristics of CH_4 and water two-phase spiral annular flow pattern in a horizontal circular tube under the condition that the guide strip rotates all the way. A three-dimensional structure is used to simulate the pipeline, and some reasonable assumptions are made to simplify the model.

(1) The fluid is incompressible.
(2) The gas−liquid two-phase temperature at the inlet is constant, there is no heat exchange process, and the energy loss in the flow process is ignored.
(3) The outlet is connected to the atmosphere, the fluid is directly discharged into the atmosphere, and the gauge pressure at the outlet is 0.
(4) The influence of pipe wall thickness and guide strip thickness on the flow pattern is neglected.

There are three kinds of multiphase flow models: the VOF model, the mixture model, and the Eulerian model. The mixture model is a model based on the assumption that the Storkes value is very small, thus simplifying the Euler method, so its calculation amount is less. The mixed model allows phase slip, that is, different initial velocities can be set for each item. It can be used for isotropic multiphase flow with strong coupling. Therefore, we can give priority to the mixture model for trial operation, and if the result is feasible, we can further consider the Eulerian model with more computation but more accuracy. After simulating several groups of experimental conditions, it was found that there is no clear phase interface with the passage of time and distance using the mixture model. The VOF model can accurately track the change in the phase interface, so it is more suitable for laminar flow and large bubble flow in a liquid. After comparing the simulation results and the applicability of the model and according to the research content of this paper, the VOF model is selected to simulate and calculate the reconstructed phase interface distribution and the change in the spiral annular flow pattern when the fluid passes through the guide strip at different gas−liquid conversion velocities.

Physical Model. *Geometric Model.* The geometric model of the entire course of diversion is shown in Figure 1. The diameter of the horizontal pipeline is D = 0.032 m and the length is L = 2 m. The guide strip is installed from the entrance, and the parameters of the diversion strip are as follows: setting angle $\theta = 25°$, height $h = D/6$, and number n = 3. The numerical simulation calculation adopts the $X-Y-Z$ three-dimensional rectangular coordinate system; the origin of the coordinate is set as the center of the entrance face of the pipeline, and the flow direction is set as the positive direction of the Z axis, flowing from the left end to the right end of the pipeline.

Boundary Conditions. Mass flow inlet is used as the boundary condition at the inlet end of the pipeline, the outlet boundary condition is outflow, and the wall surface is the nonslip wall condition. The gravity direction is the $-Y$ direction, and the acceleration of gravity is 9.81 m/s^2. The reference point is set at the outlet center of the pipeline, and the reference pressure is 0 Pa. According to the set gas−liquid mass flow rate, it is assumed that the volume fraction of each phase at the inlet is evenly distributed.

Initial Conditions. This chapter mainly simulates the flow pattern change of gas−liquid two-phase spiral annular flow under the action of the whole pipe section of the guide strip. The gas phase uses CH_4 as the medium, with a density of 0.77 kg/m^3 and a dynamic viscosity of 1.1035×10^{-5} pa s; liquid water was used as the medium, with a density of 998.2 kg/m^3 and a dynamic viscosity of 0.001003 Pa s. The flow pattern diagram[30] of the spiral flow system is shown in Figure 2. In this paper, the annular flow in the figure is simulated under different gas−liquid conversion velocities, and its parameters are selected according to the research content.

Grid Division. ICEM-CFD software was used to mesh the three-dimensional geometric model. The whole pipe adopts an

https://doi.org/10.1021/acsomega.2c02924
ACS Omega 2022, 7, 31961−31973

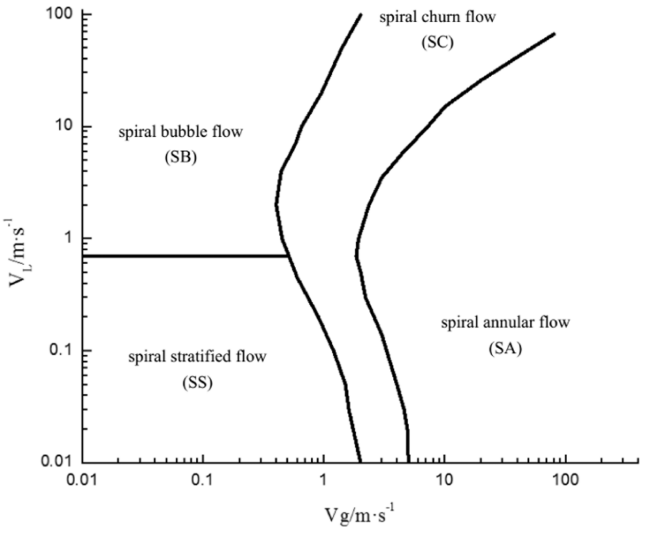

Figure 2. Gas−liquid two-phase spiral flow pattern.[30]

unstructured mesh, and the edge of the guide strip and the wall of the pipe are encrypted. The thickness of the bottom layer is 0.2 mm, and five layers are encrypted in the ratio of 1.1. The line grid is set at the intersection of the diversion channel and the wall, and the maximum size is 0.5 mm. The grid division results are shown in Figure 3.

Mathematical Model. *Control Equation.* A reasonable flow process must satisfy the conservation of mass and momentum. Because the simulation of gas−liquid two-phase flow mainly considers the change in the flow pattern and does not consider the change in the fluid temperature during the flow process, there is no need to choose the energy conservation equation.

Continuity equation

$$\frac{\partial \rho}{\partial t} + \nabla(\rho \nu) = 0 \tag{1}$$

Momentum equation

$$\frac{\rho(\varphi)\partial v}{\partial t} + \rho(\varphi)\nabla(\vec{\nu}\vec{\nu}) = -\nabla P + \mu(\varphi)\nabla\cdot[\nabla\vec{\nu} + (\nabla v)^T] + F_\sigma + \rho(\varphi)\vec{g} \tag{2}$$

where $\rho(\varphi)$ is the mixing density of two phases, kg/m^3; $\mu(\varphi)$ is the viscosity of two phases, Pa·s; P is the pressure, Pa; ν is the fluid velocity, m/s; t is time, s; and F_σ is the volume force, N.

Turbulent Motion Equation. The RNG model and the RSM model can be selected because they are two-phase flow models under the spiraling flow condition. After comparative analysis, the RSM model is selected. The RNG model is the standard k−ε model, the model has been modified, and the model is better applied to the case of a strong spiral. However, it is still limited by the assumption of isotropic vorticity in the Boussinesq method, so it cannot really reflect the change in turbulence. The RSM model is the most perfect RANS model in physics at present. It eliminates the shortcomings of the isotropic eddy viscosity assumption and can better reflect the changes of complex two-phase flow turbulence. Moreover, the RANS is the convenient computational method among the indirect turbulence simulation methods. The governing equation is as follows

$$\frac{\partial}{\partial t}(\rho\overline{u}_i'\overline{u}_i') + \frac{\partial}{\partial x_k}(\rho u_k'\overline{u}_i'\overline{u}_j') = \frac{\partial}{\partial x_k}[\frac{\nu_t \partial u_i' u_j'}{\sigma_k \partial x_k}] + P_{ij} + \varnothing_{ij} + \varepsilon_{ij} + R_{ij} + S_{ij} + D_{ij} \tag{3}$$

where

$$P_{ij} = -\rho\left[\overline{u}_i'\overline{u}_k'\frac{\partial \overline{u}_j'}{\partial xk} + \overline{u}_j'\overline{u}_k'\frac{\partial u_i'}{\partial x_k}\right] \tag{4}$$

$$\phi_{ij} = -C_1\rho\frac{\varepsilon}{K}\left[\overline{u}'_i\overline{u}'_j - \frac{2}{3}\delta_{ij}K\right] - C_2\rho\left[P_{ij} - \frac{2}{3}\delta_{ij}P\right] \tag{5}$$

$$\varepsilon_{ij} = -\frac{2}{3}\delta_{ij}\rho\varepsilon \tag{6}$$

$$R_{ij} = -2\rho\Omega_k(\overline{u}_i'\overline{u}_m'\varepsilon ikm + u_j'u_m'\varepsilon_{jkm}) \tag{7}$$

Here, C_1 and C_2 are constants; u' is the pulsation rate, m/s; ϕ is the source term; ε is the dissipation term; K is the turbulent flow energy term; v_t is the turbulent viscosity, Pa·s; x is the x axial distance, m; σ_k is a constant; Ω is a constant; $\overline{u}$ is the time mean value; i is a constant, j = 1, 2, 3; k is a constant, and m = 1, 2, 3.

CLSVOF Equation. In this paper, the CLSVOF model based on the coupling of the VOF method and the level set method is adopted. This method is widely used in the study of two-phase flow interface tracking with a complex interface. The VOF method can retain the volume conservation in calculation but cannot describe the interface curvature accurately, while the level set method can accurately describe the interface curvature and the bending effect caused by surface tension. However, the conservation of volume cannot be ensured in the calculation. Therefore, the CLSVOF model, which combines the advantages of the two models, can accurately describe the flow pattern of gas−liquid two-phase spiral flow.

VOF Model Volume Ratio Equation. The volume ratio equation is mainly not to solve the main phase but to constrain the calculation of the volume ratio as follows

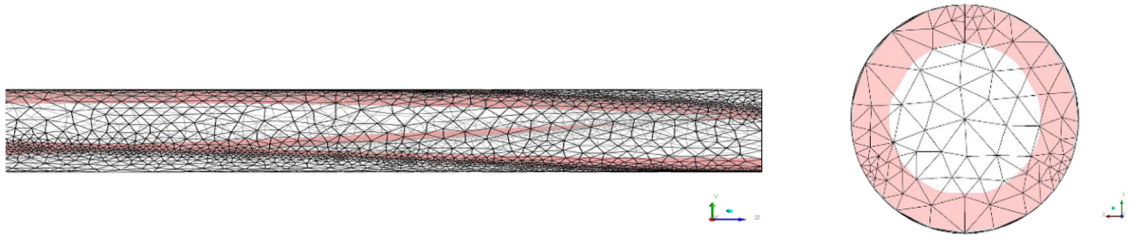

Figure 3. Mesh division.

https://doi.org/10.1021/acsomega.2c02924
ACS Omega 2022, 7, 31961−31973

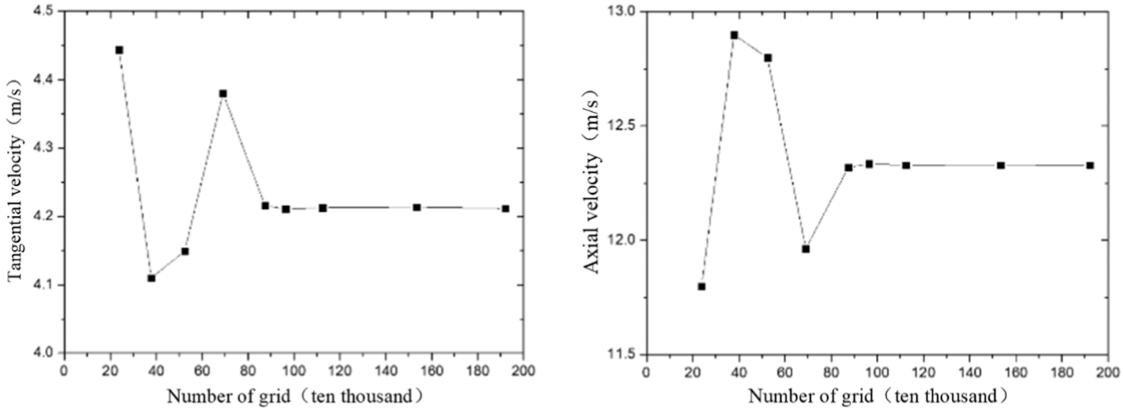

(a) Graph of tangential velocity changing with grid (b) Diagram of axial velocity changing with grid

Figure 4. Grid independence verification.

$$\frac{\partial \alpha_q}{\partial t} + \nu \nabla \alpha_q = \frac{S_{\alpha_q}}{\rho_q} \tag{8}$$

Here, α_q is the volume ratio of the q phase fluid; the right end of the equation S_{α_q} is the source item, which is zero here.

$$\sum_{q=1}^{n} \alpha_q = 1 \tag{9}$$

The basic idea of the VOF method is to define a function $(F(\Omega,t))$ about volume to characterize the volume fraction of the liquid phase in each grid cell.

$$F(\Omega, t) = \begin{cases} 1, & \text{liquid phase area} \\ 0 - 1, & \text{gas} - \text{liquid mixed phase} \\ 0, & \text{gas phase area} \end{cases} \tag{10}$$

Ω is a single grid area of the calculation.

VOF governing equation:

$$\frac{\partial F}{\partial t} + \vec{\nu} \nabla F = 0 \tag{11}$$

CLSVOF combines the level set model with the VOF model to define a function (level set function φ) to replace the VOF method. F is a function to characterize the gas−liquid interface.

Level set equation:

$$F(\Omega, t) = \begin{cases} d, & x \text{ is in the liquid phase} \\ 0, & x \text{ is in the interface} \\ -d, & x \text{ is in the gas phase} \end{cases} \tag{12}$$

φ is the level set function (distance function) and d is the shortest distance from a point to the interface x when the time is t.

The alternative way is as follows

$$F(\Omega, t) = \frac{1}{|\Omega|} \int_{\Omega} H(\varphi(x, y, t)) \mathrm{d}x\mathrm{d}y \tag{13}$$

We introduce the smoothed Heaviside function

$$H(\varphi) = \begin{cases} 1 & \varphi > \varepsilon \\ \frac{1}{2} + \frac{\varphi}{2\varepsilon} + \frac{1}{2\pi_0}{}^{1}\left[\sin\left(\frac{\pi\varphi}{\varepsilon}\right)\right] & |\varphi| \le \varepsilon \\ 0 & \varphi < \varepsilon \end{cases} \tag{14}$$

where $H(\varphi)$ represents the Heaviside function; $\varepsilon = 1.5d$; and d represents the minimum size of the grid.

$$\rho(\varphi) = \rho_g(1 - H(\varphi)) + \rho_1 H(\varphi) \tag{15}$$

$$\mu(\varphi) = \mu_g(1 - H(\varphi)) + \mu_1 H(\varphi) \tag{16}$$

Calculation Method. Numerical simulation is divided into three parts: preprocessing, calculation, and postprocessing. Preprocessing mainly includes the establishment of a physical model and grid division, in which reasonable grid division has a great influence on the calculation efficiency and the accuracy of results. The calculation mainly includes the selection of boundary conditions and initial conditions, as well as the selection of algorithms and discrete schemes. Postprocessing is carried out by CFD-Post and Tecplot; postprocessing software such as Origin analyzes the calculated date file to describe the calculated data intuitively.

Because the development of flow pattern is a dynamic process, the dynamic change and development diagram of the flow pattern at different times can be obtained by transient calculations. We set the time step to 1×10^{-5} s, and we set the calculation steps according to the approximate time required for the gas−liquid phase to complete the pipe section. The RSM model is selected as the turbulence model, and the CLSVOF method based on the pressure base is adopted as the multiphase flow model. The standard wall function is used to deal with the flow near the wall. In addition, under the condition of convergence, the pressure equation, momentum equation, turbulence kinetic energy equation, and turbulent diffusivity equation all adopt the second-order upwind scheme to improve the calculation accuracy. The volume equation adopts the Geo-Reconstruct format. Pressure−velocity coupling adopts the PISO algorithm to solve the algebraic equation discretely. The convergence condition is defined as the absolute value of the residual error $< 1 \times 10^{-6}$.

ANSYS software is used to calculate the three-dimensional transient state of the model, and the calculation data file is obtained. Then, the postprocessing software Tecplot is used to postprocess the calculated data, and the gas−liquid distribution

https://doi.org/10.1021/acsomega.2c02924
ACS Omega 2022, 7, 31961−31973

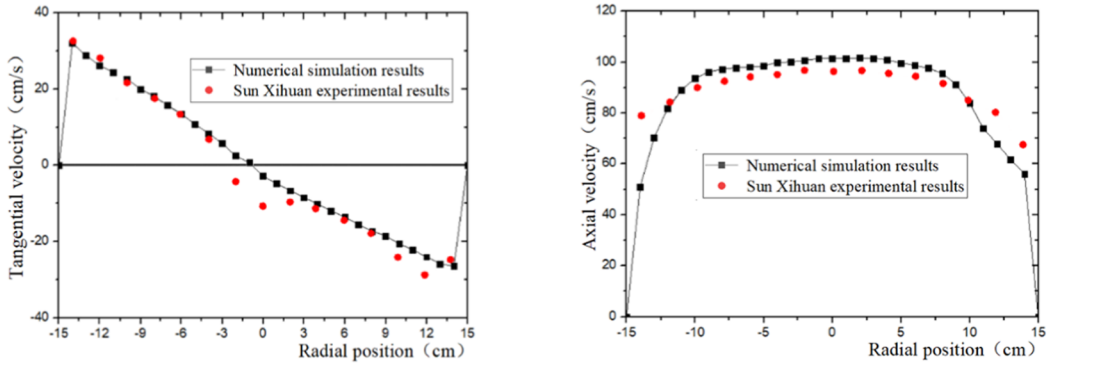

(a) Comparison diagram of tangential velocity distribution along the diameter (b) Comparison diagram of axial velocity distribution along the diameter

Figure 5. Comparison of numerical simulation and experimental result.

diagram, pressure distribution, and other specific data are obtained.

Verification of Grid Independence. To reduce the influence of grid number on the calculation results and improve the simulation efficiency, the grid number is screened by grid independence verification. Grids with the number of grids ranging from 2×10^5 to 2×10^6 are selected for simulation under the same initial and boundary conditions. The simulation results are compared according to the average axial velocity and tangential velocity in the pipe, and the results are shown in Figure 4. Through comparative analysis, it can be found that when the number of grids is greater than 8×10^5, the tangential velocity and axial velocity are less affected by the number of grids. Therefore, the grid with the number of grids about 1×10^6 is selected to ensure both high computational efficiency and high accuracy of results.

Model Feasibility Verification. The simulation results are compared with the experiments to verify the feasibility. Figure 5 is a comparison and verification diagram between simulation results and Sun's[31] experimental results. From the verification results of the simulation and the experiment, one can see that the simulation results of tangential velocity are basically consistent with the experimental results of Sun, and the asymmetric distribution of tangential velocity in numerical simulation in this paper is also consistent with the experimental results. The numerical value of the axial velocity simulation results is slightly larger than the experimental results, and its error is within an acceptable range. Therefore, in general, the numerical simulation method can be used to calculate the gas–liquid two-phase spiral annular flow in gas hydrate pipelines.

RESULTS AND DISCUSSION

Working Condition Setting. To study the flow pattern of the guide strip under the whole rotating condition, according to the flow pattern diagram of the spiral flow system studied by Rao, the gas–liquid conversion velocity was set, and 12 groups were simulated, as shown in Table 1.

Change Law of the Spiral Annular Flow Pattern. In this section, concentrating on the annular flow area in the flow pattern diagram of the spiral flow system, the numerical simulation is carried out with the guide strip rotating all the way, and three types of flow patterns are simulated, namely, spiral lump flow, spiral annular flow, and spiral annular winding flow.

Table 1. Parameter Table of Simulation Conditions

working condition	gas-phase velocity V_G (m/s)	liquid-phase velocity V_L (m/s)
1	0.01	5
2	1	1
3	1	2
4	1	4
5	1	8
6	1	10
7	1	16
8	1	24
9	2	10
10	4	10
11	6	10
12	10	10

Spiral Mass Flow. The spiral flow (SC) is shown in Figures 6–8. It can be seen that the spiral flow (SC) is characterized by the fact that the gas phase exists at the axis of the pipeline in the form of air mass or large cannonball bubbles and moves forward in a spiral way. The working condition of this flow pattern is when the ratio of the converted velocity of the liquid phase to the converted velocity of the gas phase V_L/V_G is greater than 1/2. As shown in Figures 6a, 7a, and 8a, the gas phase in the first half of the pipeline is mainly in the form of ball-shaped or cannonball-shaped bubbles, and the drag force generated by the liquid against the gas phase is reduced due to the reduction in the velocity difference between the gas and liquid phases, so the gas is divided into larger balls by the drag force. Compared with Figures 6b, 7 b, and 8b, it can be observed that with the increase in the ratio of the converted velocity of the liquid phase to the converted velocity of the gas phase V_L/V_G, the air mass in the first half of the pipeline becomes longer and longer, and the transition position of the spiral mass flow to the spiral annular winding flow in the second half of the pipeline is located more backward.

Spiral Annular Flow. The spiral flow (SA) is shown in Figures 9–11. It can be seen that the spiral flow (SA) is characterized by the fact that the gas phase generates a spiral high-speed flow in the continuous airway at the axis of the pipeline, the liquid phase forms an annular liquid film on the wall of the pipeline, and the thickness of the liquid film is larger than the height of the guide strip. The flow pattern occurs when the ratio of the liquid-phase velocity to gas-phase velocity

https://doi.org/10.1021/acsomega.2c02924
ACS Omega 2022, 7, 31961–31973

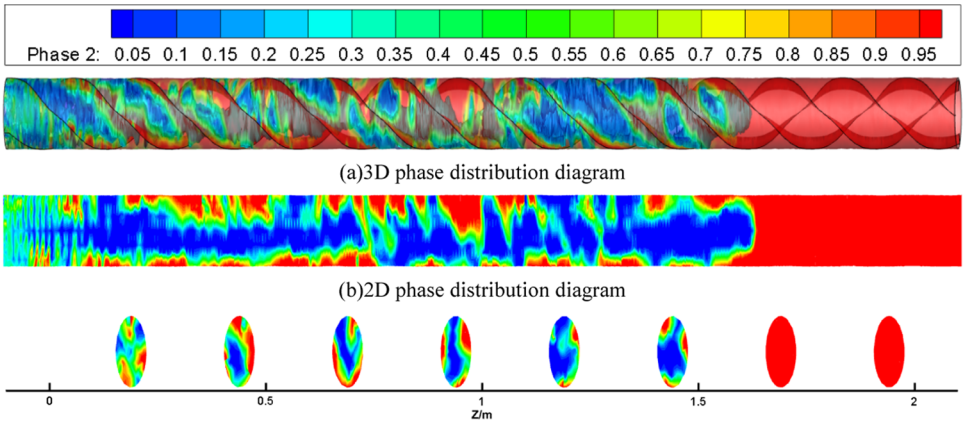

(a)3D phase distribution diagram

(b)2D phase distribution diagram

(c) Phase distribution diagram of different sections

Figure 6. V_L = 1 m/s and V_G = 2 m/s phase distribution diagrams.

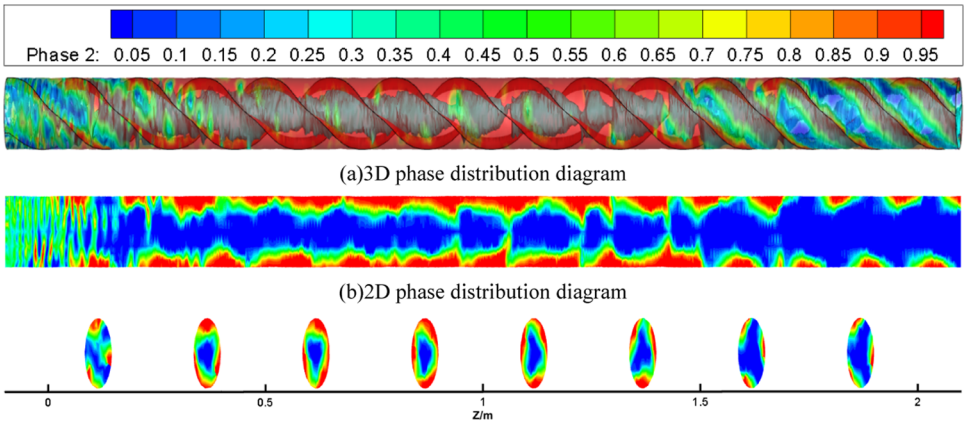

(a)3D phase distribution diagram

(b)2D phase distribution diagram

(c) Phase distribution diagram of different sections

Figure 7. V_L = 6 m/s and V_G = 10 m/s phase distribution diagrams.

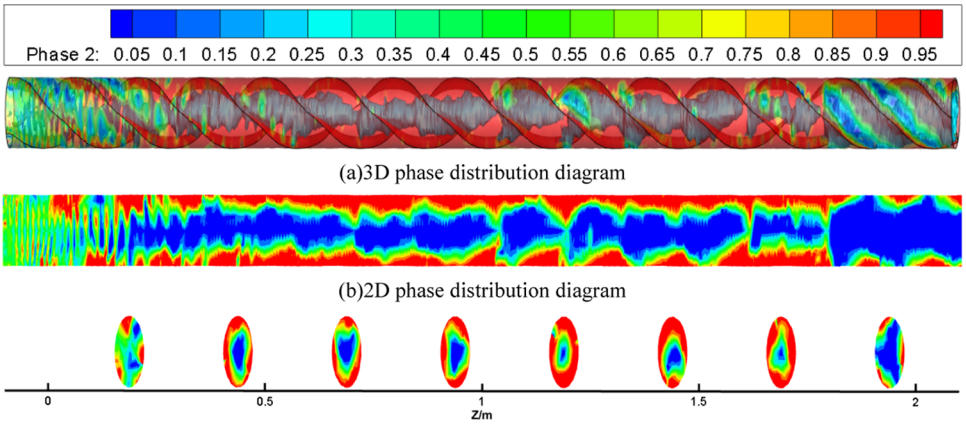

(a)3D phase distribution diagram

(b)2D phase distribution diagram

(c) Phase distribution diagram of different sections

Figure 8. V_L = 10 m/s and V_G = 10 m/s phase distribution diagrams.

V_L/V_G is in the range of 1/5 to 1/2. As the drag force is less than the surface tension of the gas−liquid interface, the gas phase exists as a continuous phase, as shown in the first half of the pipeline in Figures 9a, 10a, and 11a. Comparing Figures 9b, 10b, and 11b, it is found that with the increase in the ratio of the liquid-phase velocity to the gas-phase velocity V_L/V_G, the occurrence area of spiral annular flow also increases and the diameter of spiral air flow also increases. From Figures 9c, 10c, and 11c, it can be seen that the specific gravity of the liquid phase in the first half of the pipe section is larger than that of spiral annular winding flow in the second half.

Spiral Annular Winding Flow. The spiral wound flow (SAT) is shown in Figures 12−15. Compared with the spiral wound flow (SA), the difference in the spiral wound flow (SAT) is that there is no continuous liquid film on the pipe wall, and the thickness of the liquid film is smaller than the

https://doi.org/10.1021/acsomega.2c02924
ACS Omega 2022, 7, 31961−31973

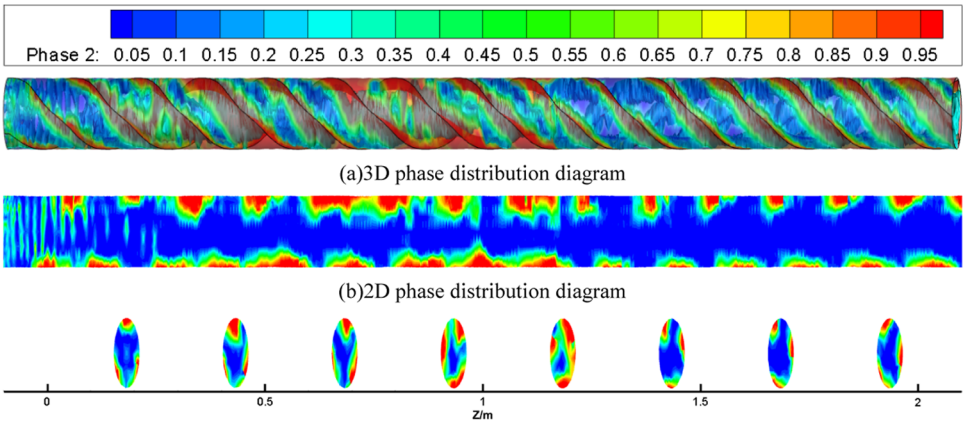

(a)3D phase distribution diagram

(b)2D phase distribution diagram

(c) Phase distribution diagram of different sections

Figure 9. V_L = 1 m/s and V_G = 4 m/s phase distribution diagrams.

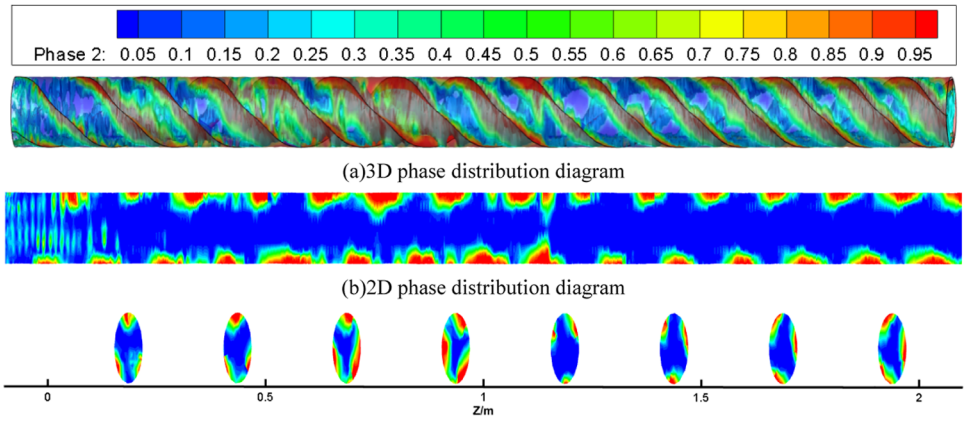

(a)3D phase distribution diagram

(b)2D phase distribution diagram

(c) Phase distribution diagram of different sections

Figure 10. V_L = 2 m/s and V_G = 10 m/s phase distribution diagrams.

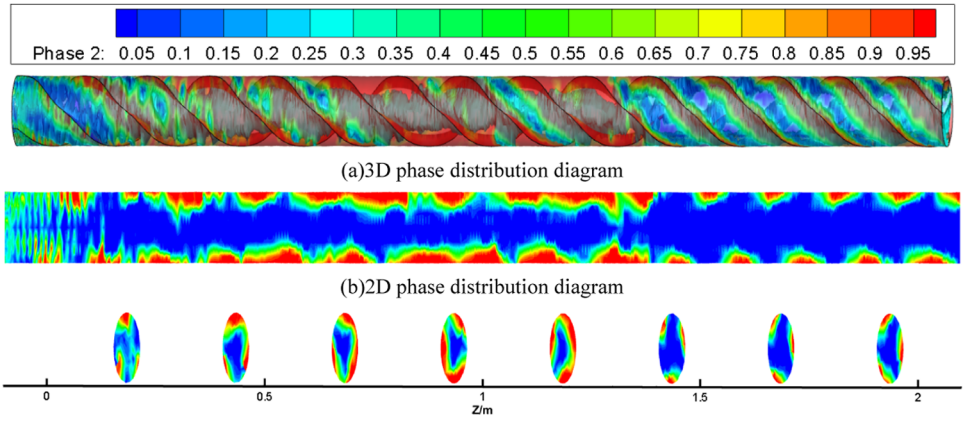

(a)3D phase distribution diagram

(b)2D phase distribution diagram

(c) Phase distribution diagram of different sections

Figure 11. V_L = 4 m/s and V_G = 10 m/s phase distribution diagrams.

height of the guide strip. The liquid phase is divided into three paths by the guide strip and flows forward in a spiral way along the windward and leeward sides of the guide strip. A new gas channel appears between the two guide strips. The flow pattern occurs when the ratio of the liquid-phase velocity to gas-phase velocity V_L/V_G is less than 1/5, as shown in the whole pipe section of Figures 12a, 13a, 14a, and 15a. Comparing Figures 12b, 13b, 14b, and 15b, it is found that with the decrease in the ratio of the liquid-phase velocity to gas-phase velocity V_L/V_G, the range of gas-phase gas passages between the flow guide strips becomes larger.

Effect of Gas−Liquid Two-Phase Conversion Velocity on Flow Pattern. *Influence of Gas-Phase Converted Velocity on Flow Pattern.* Table 2 shows the effect of gas-phase converted velocity on flow pattern conversion under the condition of full rotation of the guide strip. It can be seen from

https://doi.org/10.1021/acsomega.2c02924
ACS Omega 2022, 7, 31961−31973

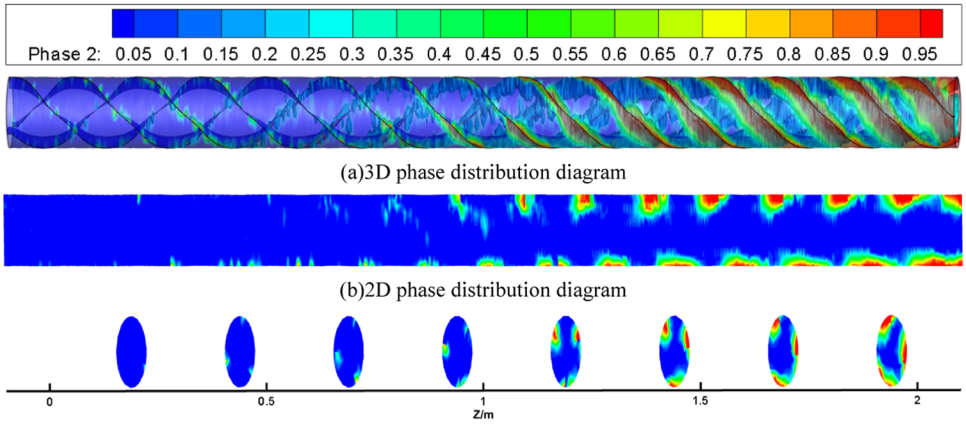

(a)3D phase distribution diagram

(b)2D phase distribution diagram

(c) Phase distribution diagram of different sections

Figure 12. V_L = 0.01 m/s and V_G = 5 m/s phase distribution diagrams.

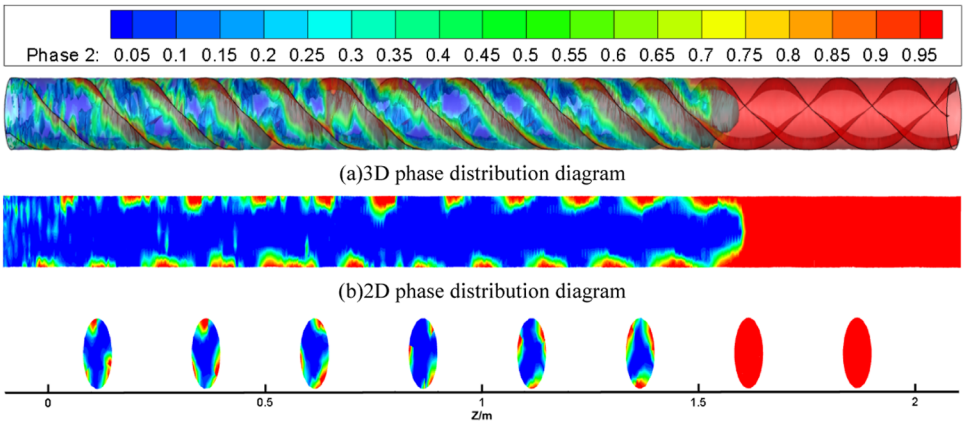

(a)3D phase distribution diagram

(b)2D phase distribution diagram

(c) Phase distribution diagram of different sections

Figure 13. V_L = 1 m/s and V_G = 8 m/s phase distribution diagrams.

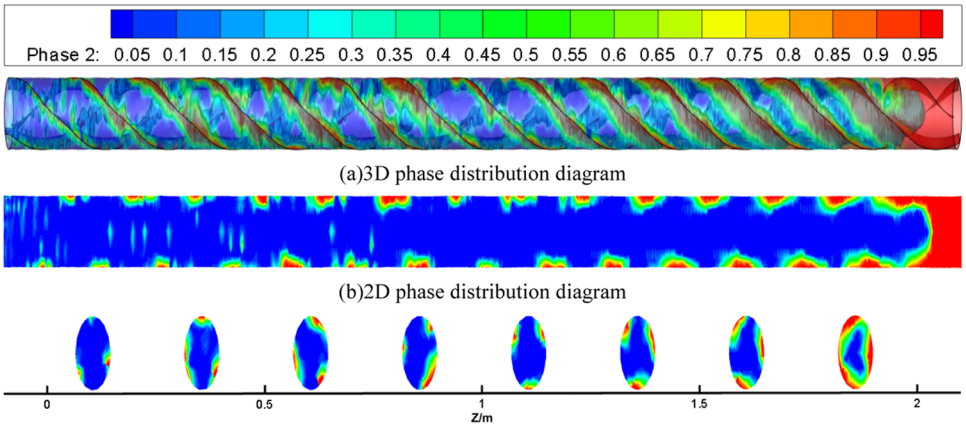

(a)3D phase distribution diagram

(b)2D phase distribution diagram

(c) Phase distribution diagram of different sections

Figure 14. V_L = 1 m/s and V_G = 16 m/s phase distribution diagrams.

the table that spiral annular winding flow (SAT) occurs in all pipe sections, and the larger the gas velocity is, the larger the range of spiral annular winding flow appears. In the first half of the pipeline, with the increase in gas-phase conversion velocity, the flow pattern transits from spiral mass flow (SC) to spiral annular flow (SA), Finally, it becomes spiral annular winding flow (SAT). The reason for this flow pattern transition is that when the ratio of the liquid-phase velocity to gas-phase velocity V_L/V_G is greater than 1/2, the gas phase mainly exists in the form of air mass due to the drag force generated by the velocity slip liquid relative to the gas phase, and the spiral mass flow (SC) is caused by the tangential force generated by the spiral flow of the liquid phase. With the increase in gas-phase velocity, the velocity ratio of the liquid phase to the gas phase decreases, the specific gravity of gas increases, and the water content decreases at the same cross section. The drag force

https://doi.org/10.1021/acsomega.2c02924
ACS Omega 2022, 7, 31961−31973

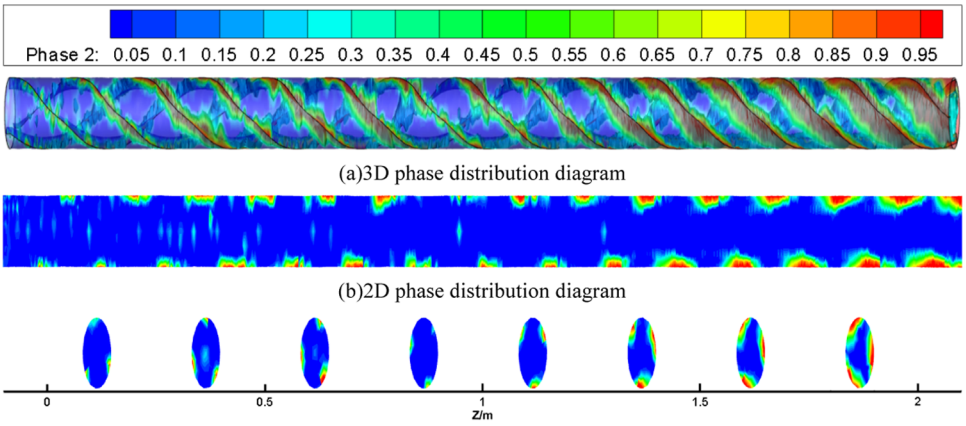

Figure 15. V_L = 1 m/s and V_G = 24 m/s phase distribution diagrams.

Table 2. Influence of Gas Velocity Change on Flow Pattern

conversion rate of liquid phase V_L (m/s)	gas-phase conversion velocity V_G (m/s)	liquid-phase and gas-phase velocity V_L/V_G	spiral mass flow (m)	spiral flow (m)	spiral wound flow (m)
1	2	1/2	0−1		1−2
	4	1/4		0−1.25	1.25−2
	8	1/8			0−2
	16	1/16			0−2
	24	1/24			0−2

caused by velocity slip changes into the action of gas against the liquid phase, and the gas phase exists continuously through the airway at the axis, while the liquid phase forms an annular liquid film on the pipe wall due to centrifugal force. When the gas-phase velocity is further increased, on the same cross section, the specific gravity of the gas increases again, and the airway gradually expands from the axis to the wall of the pipe, and the thickness of the liquid film of the liquid phase becomes thinner due to the expansion of the airway. When the velocity ratio of the liquid phase to the gas phase V_L/V_G is less than 1/5, the thickness of the liquid film is smaller than the height of the guide strips, the liquid film is cut by the guide strips, and a new airway is formed between the two guide strips and connected with the original airway. Thus, the liquid phase tightly clings to the windward side and the leeward side of the guide strip to flow in a spiral winding manner.

Effect of Liquid-Phase Conversion Velocity on Flow Pattern. Table 3 shows the effect of liquid-phase conversion velocity on the flow pattern conversion under the condition of full rotation of the guide strip. It can be seen from the table that when the conversion speed of the gas phase is constant, the increasing conversion speed of the liquid phase will cause the position of spiral annular winding flow (SAT) in the second half of the pipeline to gradually move backward. In the first half of the pipeline, as the velocity ratio of the liquid phase to the gas phase V_L/V_G increases, the type I flow transits from spiral annular winding flow (SAT) to spiral annular flow (SA) and finally to spiral mass flow (SC). When the gas-phase velocity is high and V_L/V_G is less than 1/5, the drag force caused by the velocity slip between the gas phase and the liquid phase is in the form of a gas phase acting on the liquid phase, and the liquid film thickness is smaller than the height of the guide strips due to the expansion of the air channel, and an air channel appears between the two guide strips. Therefore, a spiral annular winding flow (SAT) is formed in the whole pipe section. However, when the conversion speed of the liquid phase increases, the speed ratio of the liquid phase to the gas phase V_L/V_G also increases, the drag force generated by the gas phase to the liquid phase gradually decreases, the liquid film thickness of the liquid phase increases, the airway between guide strips disappears, and the gas phase only flows continuously at the axis of the pipeline. At this time, the spiral annular flow (SA) appears. With the further increase of liquid phase velocity, the velocity ratio of the liquid phase to the gas phase decreases again, the liquid content on the same cross section becomes larger, and the form of drag force changes into a liquid phase acting on the gas phase. The gas phase is torn by the liquid phase due to the low tension and is dispersed in the liquid phase into ball-shaped or cannonball-shaped bubbles, so spiral ball-shaped flow (SC) appears.

Table 3. Influence of Liquid Velocity Change on Flow Pattern

gas-phase conversion velocity V_G (m/s)	conversion rate of liquid phase V_L (m/s)	liquid-phase and gas-phase velocity V_L/V_G	spiral mass flow (m)	spiral flow (m)	spiral wound flow (m)
10	1	1/10			0−2
	2	1/5		0−1.1	1.1−2
	4	2/5		0−1.3	1.3−2
	6	3/5	0−1.5		1.5−2
	10	1	0−1.75		1.75−2

Comparison of Spiral Annular Flow under Different Spinning Modes. Figure 16 shows the spiral annular flow produced by different spinning modes. It can be seen from the figure that, because the number of spiraling flows in the rotating pipe of the twisted tape is continuously declining, the liquid phase gathers at the bottom of the pipe under the action of gravity, the gas phase gradually rises above the pipe, the gap between the thickness of the liquid film at the bottom of the pipe and the top of the pipe gradually widens, and the spiral annular flow tends to become a stratified flow. However, the spiral annular flow formed under the whole rotating condition of the guide strip exists in two forms: annular flow and annular winding flow, and the liquid-phase flow form of annular

https://doi.org/10.1021/acsomega.2c02924
ACS Omega 2022, 7, 31961−31973

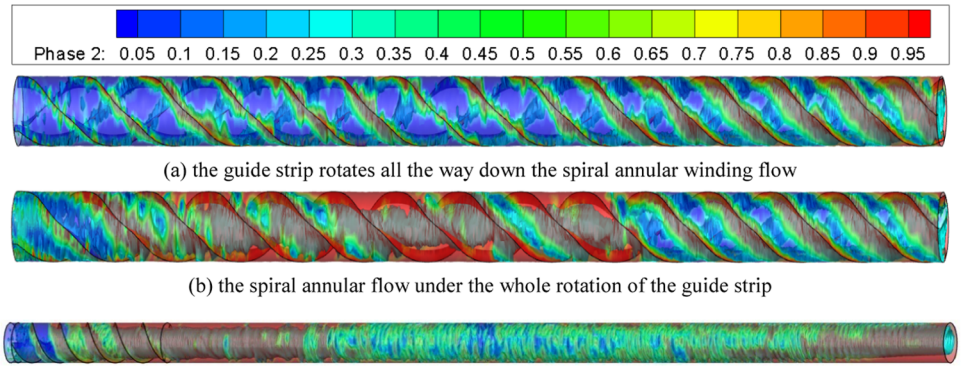

(a) the guide strip rotates all the way down the spiral annular winding flow

(b) the spiral annular flow under the whole rotation of the guide strip

(c) Spiral annular flow under the local rotation of the twisted tape.

Figure 16. Comparison of spiral annular flow under different spin modes.

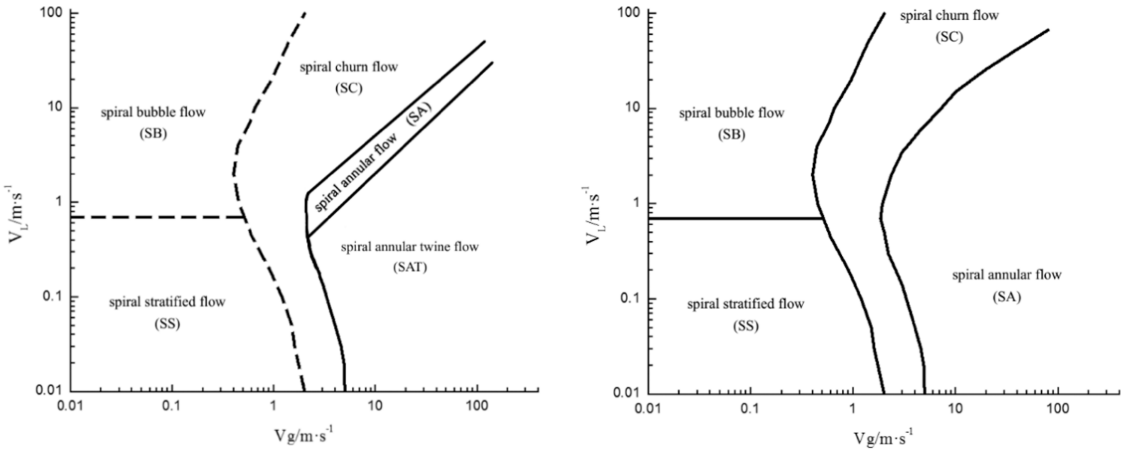

(a) Flow pattern diagram of spiral flow with the guide strip by spiral on-way

(b) Flow pattern diagram of spiral flow under local rotation of twisted tape [30]

Figure 17. Comparison of flow patterns in different spiral modes.

winding flow is consistent with the hydrate particle flow form of the gas−solid two-phase flow mentioned above, which can provide a theoretical basis for the gas−liquid−solid three-phase flow of hydrates.

Flow Pattern Diagram. We select the flow pattern of the first half of the pipeline to draw the flow pattern diagram of the whole rotating system of the guide strip and compare it with the spiral flow pattern diagram of Rao[30] under the partial rotation of the short twisted tape, as shown in Figure 17. Rao[30] believes that when the gas−liquid two-phase velocity ratio V_L/V_G is greater than 1 under the local spinning condition, a drag force will be generated. When the drag force cannot offset the surface tension on the interface, the gas phase will appear in the form of mass flow or annular flow. However, when the velocity ratio of the liquid phase to the gas phase $V_L/V_G > 1/2$, the drag force appears under the simulated condition of the whole rotation of the deflector. Comparing Figure 17a with Figure 17b, it is found that (1) the boundary of the transformation from lumpy flow (SC) to annular flow (SA) is delayed. Because of the different working conditions of spinning, under the whole rotating condition of the deflector, the drag force appears when the velocity ratio of the liquid phase to the gas phase $V_L/V_G > 1/2$. When the drag force is greater than the surface tension, the gas phase cannot keep the original stable airway, the gas−liquid interface is destroyed, and the continuous airway is transformed into air mass. (2) A new flow pattern, annular winding flow (SAT), is derived from annular flow under the condition that the guide strip rotates all the way. When the velocity ratio of the liquid phase to the gas phase V_L/V_G is less than 1/5, the liquid film thickness of the liquid phase gradually becomes thinner. When it is less than the height of the guide strip, the liquid film is cut by the guide strip, and a new air passage appears between the two guide strips, so the liquid phase can only flow close to the guide strip.

CONCLUSIONS

In this paper, the RSM k-ε model and the level set model under the VOF method are used to simulate the annular flow region in the downward flow pattern of the spiral flow system, and the following conclusions are obtained.

a. Three main flow patterns are obtained by simulation, namely, spiral mass flow, spiral annular flow, and spiral annular winding flow. The flow pattern characteristics of spiral gas−liquid two-phase flow are introduced.

b. The velocity ratio of the liquid phase to the gas phase V_L/V_G is the main factor that affects the existing form of the gas phase. When $V_L/V_G > 1/2$, the gas phase is broken by the liquid phase and is divided into lumps. When $1/5 < V_L/V_G < 1/2$, the drag force cannot be

https://doi.org/10.1021/acsomega.2c02924
ACS Omega 2022, 7, 31961−31973

achieved. A new airway appears between the two guide strips.

c. According to the simulation results, the flow pattern of the gas−liquid two-phase spiral flow under the condition of full rotation of the guide strip is drawn, and compared with the flow pattern of Rao's short twisted tape with local rotation, it is found that the occurrence condition of annular flow is delayed. This is mainly due to the fact that when $V_L/V_G > 1/2$, the unreduced drag force of the spiral flow still acts on the gas phase, and the gas phase is torn by the liquid phase and divided into clusters. The new flow pattern is derived from the annular flow, mainly because the gas phase velocity increases and the liquid film of the annular flow become thinner. When the liquid film is lower than the height of the guide strip, it is cut by the guide strip, so that the liquid phase flows near the guide strip.

AUTHOR INFORMATION

Corresponding Author

Shuli Wang − *School of Energy, Quanzhou Vocational and Technical University, Quanzhou, Fujian 362268, China*; Email: wsl@cczu.edu.cn

Authors

Yongchao Rao − *Jiangsu Key Laboratory of Oil-Gas Storage and Transportation Technology, Changzhou University, Changzhou, Jiangsu 213164, China; School of Petroleum Engineering, Changzhou University, Changzhou, Jiangsu 213164, China;* orcid.org/0000-0003-4933-7758

Lijun Li − *China Petroleum & Chemical Corporation North China Oil & Gas Company, Zhengzhou, Henan 450006, China*

Complete contact information is available at: https://pubs.acs.org/10.1021/acsomega.2c02924

Notes

The authors declare no competing financial interest.

The data presented in this study are available on request from the corresponding author.

ACKNOWLEDGMENTS

This work was supported by the National Nature Science Foundation of China (No. 51574045), the CNPC Innovation Foundation (No. 2020D-5007-0211), the General Project of Natural Science Research in Jiangsu Universities (No. 22KJB440002), the Changzhou Applied Basic Research Project (No. CJ20200085), the Vice General Project of Science and Technology of Jiangsu Province (No. FZ20211199), and the Opening Fund of Jiangsu Key Laboratory of Oil-gas Storage and Transportation Technology (No. CDYQCY202105).

REFERENCES

(1) Manglik, R. M.; Bergles, A. E. Swirl flow heat transfer and pressure drop with twisted-tape inserts. *Adv. Heat Transfer* **2003**, *36*, 183−265.

(2) Li, W. D.; Li, R. X.; Zhou, L. X. Liquid layer and disturbance waves properties in horizontal annular flow. *J. Tsinghua Univ.* **2000**, *40*, 23−26.

(3) Zhou, Y. L.; Zhang, L. Y. Numerical Simulation of Gas-Liquid Two-Phase Flow Pattern Conversion in a Rectangular Section of a Spiral Pipe. *J. Chem. Ind. Eng.* **2014**, *6*, 4767−4774.

(4) Rao, Y. C.; Sun, Y.; Wang, S. L.; Jia, R. Numerical simulation atudy on the law of attenuation of hydrate particles in a gas transmission pipeline. *Energies* **2019**, *12*, 58−67.

(5) Rao, Y. C.; Wang, Z. W.; Wang, S. L.; Yang, M. G. Investigation on gas hydrate slurry pressure drop properties in a spiral flow loop. *Energies* **2018**, *11*, 1384−1395.

(6) Cai, B.; Xia, G. D.; Yang, G. Study on Flow Pattern and Pressure Drop Characteristics of Gas-Liquid Two-Phase Flow in Screw Channel. *J. Eng. Therm.* **2016**, *37*, 1690−4774.

(7) Liu, X. F.; Xia, G. D.; Yang, G. Experimental study on the slug flow in a spiral channel with rectangular cross section. *J. Chem. Ind. Eng.* **2016**, *37*, 1690−4774.

(8) Liu, S. L.; Cai, W. H.; Li, F. C. Numerical Simulation of Flow Pattern and Heat Transfer Characteristics of Vapor-Liquid Two-Phase Flow in Horizontal Pipe. *J. Eng. Therm.* **2014**, *46*, 57−64.

(9) Cui, W. Z.; Li, L. J.; Xin, M. D.; et al. An experimental study of flow pattern and pressure drop for flow boiling inside microfinned helically coiled tube. *Int. J. Heat Mass Transfer* **2008**, *51*, 169−175.

(10) Subhashini, V.; Nigam, K. D. P. Experimental investigation of void fraction and flow pattern coiled flow inverter. *Chem. Eng. Process.* **2008**, *47*, 1281−1291.

(11) Liu, X. F.; Xia, G. D.; Yang, G. Experimental study on the characteristics of air−water two-phase flow in vertical helical rectangular channel. *Int. J. Multiphase Flow* **2015**, *73*, 227−237.

(12) Kanizawa, F. T.; Gherhardt, R. Two-phase flow patterns and pressure drop inside horizontal tubes containing twisted-tape inserts. *Int. J. Multiphase Flow* **2012**, *47*, 50−65.

(13) Wang, S. L.; Rao, Y. C.; Wu, Y. X.; Zhou, S. D.; Sun, L. Experimental study on gas-liquid spiral flow with twisted types. *J. Hydrodyn.* **2013**, *28*, 105−110.

(14) Wang, S. L.; Rao, Y. C.; Wu, Y. X.; Wang, X. B. Experimental research on gas-liquid two-phase spiral flow in horizontal pipe. *China Pet. Process. Petrochem. Technol.* **2012**, *14*, 24−32.

(15) Rao, Y. C.; Wang, S. L.; Zhou, S. D.; Li, E. T.; Liu, W. M. Experimental research on velocity distribution and attenuation characteristic of spiral flow by LDV. *ASME J. Fluids Eng.* **2014**, *136*, 1−9.

(16) Rao, Y. C.; Ding, B. Y.; Wang, S. L.; et al. Flow pattern and pressure drop of gas-liquid two-phase swirl flow in a horizontal pipe. *J. Central South Univ.* **2019**, *26*, 2528−2542.

(17) Wang, S. L.; Ding, B. Y.; Rao, Y. C.; Chen, F. Study on the influence of coconut oil on flow pattern and pressure drop of two-phase swirl flow. *RSC Adv.* **2019**, *9*, 32644−32655.

(18) Liu, W.; Lv, X. F.; Bai, B. F. Axial development of air−water annular flow with spiral in a vertical pipe. *Int. J. Multiphase Flow* **2020**, *124*, No. 103165.

(19) Liu, W.; Lv, X. F.; Bai, B. F. The effect of spiral on transition from churn flow to annular flow in an intermediate diameter pipe. *Exp. Therm. Fluid Sci.* **2019**, *109*, No. 109861.

(20) Cui, W. Z.; Xin, M. D. Annular flow heat transfer correlation of R134a evaporating inside three-dimensional microfin helical coiled tube. *J. Therm. Sci. Technol.* **2003**, *2*, 226−229.

(21) Zeng, X. W.; Sun, Q. G.; Lv, H. B. Research on Annular Flow Forming in Gas oil Lubrication Pipe and Affecting Factors. *Mach. Build. Autom.* **2014**, *43*, 60−62.

(22) Fang, Z. J.; Liang, F. C.; Xie, Z. Q. Gas-liquid Two-phase Annular Flow Numerical Simulation and Flow Rate Measurement Based on Centrifuge Method. *Sci. Technol. Eng.* **2017**, *17*, 1−4.

(23) Rao, Y. C.; Sun, Y.; Ding, B. Y.; Wang, S. L.; Ge, H.; Ding, B.; Yang, M. G. Investigation on gas hydrate formation properties in a spiral flow using a flow loop. *Int. J. Oil Gas Coal Technol.* **2020**, *25*, 292−318.

(24) Kanizawa, F. T.; Ribatski, G. Two-phase flow patterns and pressure drop inside horizontal tubes containing twisted-tape inserts. *Int. J. Multiphase Flow* **2012**, *47*, 50−65.

(25) Raeiszadeh, F.; Hajidavalloo, E.; Behbahaninejad, M.; Hanafizadeh, P. Effect of pipe rotation on downward co-current air-water flow in a vertical pipe. *Int. J. Multiphase Flow* **2016**, *81*, 1−14.

(26) Baghernejad, Y.; Hajidavalloo, E.; Hashem Zadeh, S. M.; Zadeh, S. M. Effect of piperotation on flow pattern and pressure drop of horizontal two-phase flow. *Int. J. Multiphase Flow* **2019**, *111*, 101−111.
(27) Liu, W.; Jiang, S.; Li, H. Z. Experimental study of liquid-carrying by swirling flow in a U-shaped tube. *Exp. Therm. Fluid Sci.* **2022**, *130*, No. 110479.
(28) Rao, Y. C.; Li, L. J.; Wang, S. L.; Zhao, S.; Liu, Z. H. Numerical Simulation Study on Flow Laws and Heat Transfer of Gas Hydrate in the Spiral Flow Pipeline with Long Twisted Band. *Entropy* **2021**, *23*, No. 489.
(29) Rao, Y. C.; Liu, Z. H.; Wang, S. L.; Li, L. J. Numerical Simulation of Spiral Flow Characteristics of CO2 Hydrate Slurry by Short Twisted Band. *Entropy* **2021**, *23*, No. 913.
(30) Rao, Y. C.; Li, L. J.; Wang, S. L.; Liu, Z. H. Numerical Simulation on the Flow Pattern of a Gas-Liquid Two-Phase Spiral Flow. *ACS Omega* **2022**, *7*, 2679−2689.
(31) Sun, X. H.; Yan, Q. L.; Li, Y. Y. *Study on Hydraulic Characteristics of Spiral Flow Pipeline Transportation*; China Water Resources and Hydropower Press: Beijing, 2012.

https://doi.org/10.1021/acsomega.2c02924
ACS Omega 2022, 7, 31961−31973